iScience

CellPress
OPEN ACCESS

Article

Engineering probiotic-derived outer membrane vesicles as functional vaccine carriers to enhance immunity against SARS-CoV-2

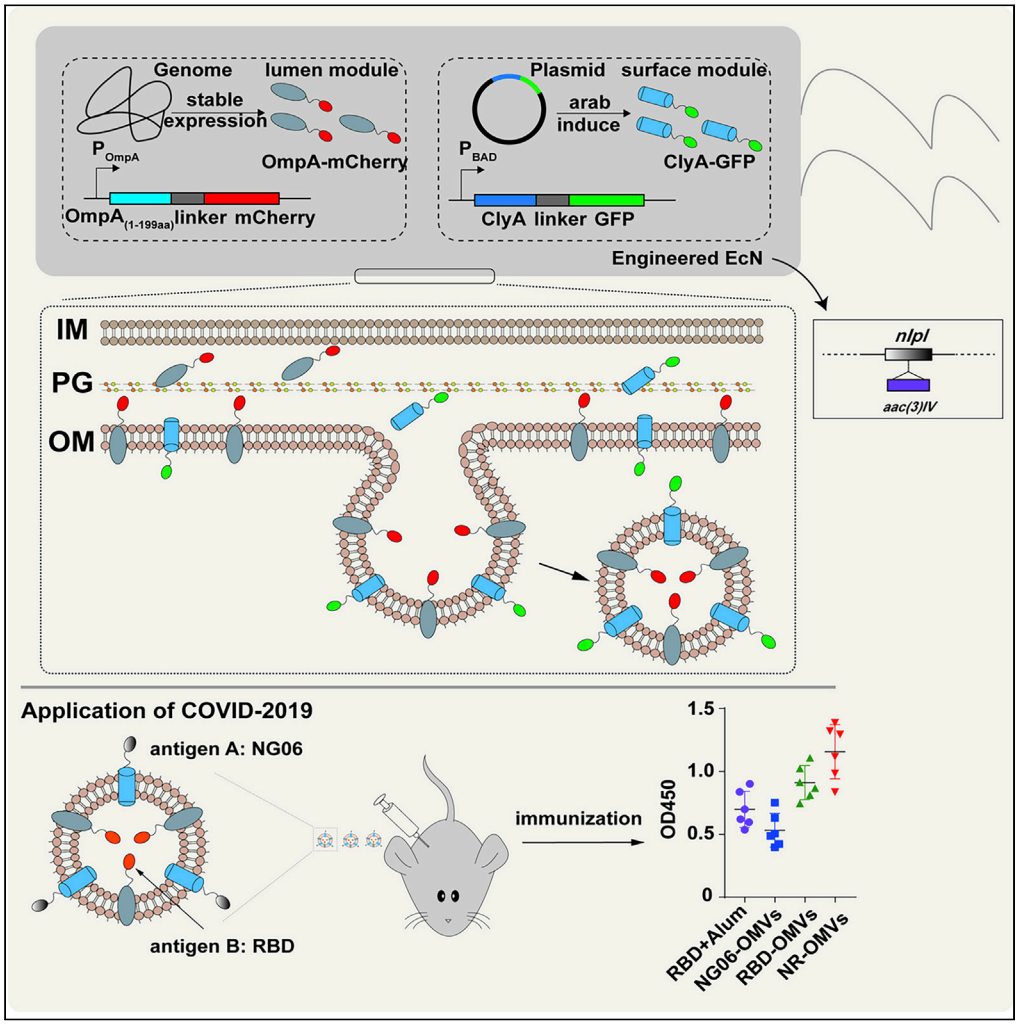

Jing Wo, Zhao-Yong Lv, Jia-Nan Sun, Hao Tang, Nan Qi, Bang-Ce Ye

bcye@ecust.edu.cn

Highlights

We used OMVs to co-express heterologous antigens in their functional conformation

RBD-OMVs triggered the activation of immune responses against SARS-CoV-2

NG06 decorations on the RBD-OMV surface induced high IgG titers against RBD

Periplasmic expression favors antigens' disulfide bond formation and correct folding

Wo et al., iScience 26, 105772
January 20, 2023
https://doi.org/10.1016/j.isci.2022.105772

iScience

CellPress
OPEN ACCESS

Article

Engineering probiotic-derived outer membrane vesicles as functional vaccine carriers to enhance immunity against SARS-CoV-2

Jing Wo,[1,3] Zhao-Yong Lv,[1,3] Jia-Nan Sun,[1] Hao Tang,[1] Nan Qi,[1] and Bang-Ce Ye[1,2,4,*]

SUMMARY

Because of the continued emergence of SARS-CoV-2 variants, there has been considerable interest in how to display multivalent antigens efficiently. Bacterial outer membrane vesicles (OMVs) can serve as an attractive vaccine delivery system because of their self-adjuvant properties and the ability to be decorated with antigens. Here we set up a bivalent antigen display platform based on engineered OMVs using mCherry and GFP and demonstrated that two different antigens of SARS-CoV-2 could be presented simultaneously in the lumen and on the surface of OMVs. Comparing immunogenicity, ClyA-NG06 fusion and the receptor-binding domain (RBD) of the spike protein in the OMV lumen elicited a stronger humoral response in mice than OMVs presenting either the ClyA-NG06 fusion or RBD alone. Taken together, we provided an efficient approach to display SARS-CoV-2 antigens in the lumen and on the surface of the same OMV and highlighted the potential of OMVs as general multi-antigen carriers.

INTRODUCTION

Outer membrane vesicles (OMVs) are natural non-replicating entities released from the outer membrane of Gram-negative bacteria with sizes ranging from 20 to 250 nm.[1,2] The OMV membrane is enveloped with extracellular membrane proteins, phospholipid, and lipopolysaccharides, and the lumen of the vesicle contains nucleic acid material, enzymes, virulence factors, and other molecules derived from parental strains.[3,4] The emergence of OMVs as a promising vaccine platform is attributed to four key features. Importantly, agonists or pathogen-associated molecular patterns (PAMPs) on the surface of OMVs exhibited activating intrinsic and adaptive immunity as their originated bacterium. The OMV nano-sized structure facilitates immune stimulation.[5,6] Also, OMVs are non-replicative nanoparticles, and their isolation does not require treatment with deactivating agents, thus preserving the native state of antigens. Furthermore, the procedure of OMV purification is relatively simple. OMVs can be obtained from the culture supernatant by ultracentrifugation. In addition, OMVs can be decorated with foreign proteins by using different synthetic biology approaches.[7] For instance, OMVs displaying ClyA-M2e4xHet, an influenza A-based peptide, gave 100% protection from a lethal challenge with two influenza A virus strains (H1N1 and H3N2) in mice.[8] Although engineered OMVs are successfully used as single antigens carriers, the research on the co-expression of more than one antigen in the same OMV is limited.

OMVs can be loaded with heterologous antigens by directing protein expression onto the outer membrane or into the lumen.[7] Surface display efficiently targets heterologous antigens to the OMV surface by fusing the foreign protein with native OMV proteins. The bacterial hemolysin ClyA is one of the best-described carrier proteins.[9] By fusing GFP with ClyA, Chen et al. expressed GFP on the OMV surface and induced an immune response.[10] The autotransporter Hbp is another class of carriers developed to load three antigen fragments on the OMV surface.[11] As an alternative for surface display, heterologous antigens can be delivered and accumulated in the OMV lumen via periplasmic expression. Fantappie et al. expressed heterologous antigens in their functional conformation in the OMV lumen and elicited robust immune responses.[12]

Here, we selected and compared three classical OMV lumen presentation patterns using red fluorescent protein (mCherry) as the model antigen, and the data showed that the fluorescence intensity of the OmpA (1–199 aa)-mCherry fusion pattern was the highest. Then, we successfully built a dual antigen presentation

[1]Institute of Engineering Biology and Health, Collaborative Innovation Center of Yangtze River Delta Region Green Pharmaceuticals, College of Pharmaceutical Sciences, Zhejiang University of Technology, Hangzhou 310014 Zhejiang, China

[2]Lab of Biosystem and Microanalysis, State Key Laboratory of Bioreactor Engineering, East China University of Science and Technology, Shanghai 200237, China

[3]These authors contributed equally

[4]Lead contact

*Correspondence: bcye@ecust.edu.cn

https://doi.org/10.1016/j.isci.2022.105772

OMV platform by anchoring green fluorescent protein (GFP) to the surface of OMVs by fusion with ClyA. The receptor-binding domain (RBD) of SARS-CoV-2 was incorporated into the OMV lumen in functional conformation to test the feasibility and effectiveness of this platform. NG06, the fragment of RBD, was loaded on the surface of RBD-OMVs to generate an enhanced vaccine candidate NR-OMV. Mice vaccinated with NR-OMVs elicited stronger specific humoral immune responses than either NG06-OMVs or RBD-OMVs.

RESULTS

The mCherry directed to the periplasm of *Escherichia coli* Nissle 1917 was internalized into the OMV lumen

According to the outer membrane vesicle generation mechanism, periplasmic proteins are naturally wrapped into the lumen of OMVs, therefore, the target antigen can be displayed in the OMV lumen by using the secreted protein signal peptide in the periplasm.[13] Here, by testing the fluorescence intensity of mCherry, we compared the efficiency of three luminal expression patterns. Outer membrane protein A family (OmpA) is a group of porin proteins with a high-copy number in the outer membrane of Gram-negative bacteria.[14] The N-terminal domain of OmpA forms an anti-parallel β barrel structure by eight transmembrane strands, facilitating embedded in the outer membrane.[15] The C-terminal domain of OmpA, which is connected to the peptidoglycan layer, is globular and located in the periplasmic space.[15] Therefore, foreign antigens replacing the C-terminus of OmpA, fused with the OmpA-β-barrel region, can be spontaneously wrapped into the OMV.

Furthermore, the accumulation of foreign antigens in the lumen of OMVs can be achieved by fusing the signal peptide of OmpA proteins.[12,16] The difference between these two approaches is that the fusion of a signal peptide leads to free floating protein in the periplasm, whereas fusion to the OmpA C-terminus leads to an outer-membrane bound protein that extends into the periplasm. In addition, expressing the target antigen as a lipoprotein is an alternative for OMV loading foreign antigens in the lumen.[17] In Gram-negative bacteria, a nascent lipoprotein consists of an N-terminal leader sequence following a cysteine-containing "lipobox." After processing, the mature lipoprotein is translocated to the periplasmic side of the outer membrane by its acylated cysteine.[18,19] In *Escherichia coli*, Braun's lipoprotein (Lpp) accounts for about a million copies per cell and is the most abundant protein.[17] Theoretically, the fusion of the RBD coding sequences to the lipobox of the Lpp leader sequence is an efficient way to express heterologous proteins in the OMV lumen. Foreign antigens disrupt the adhesion of OmpA to the peptidoglycan layer, which makes the association between the outer membrane and peptidoglycan weaker and promotes a higher yield of OMV.[1]

To obtain consistently stable engineered OMVs and avoid the addition of different inducers during the procedure, we designed three fusion expression patterns, including OmpA-SP-mCherry, LPP-SP+C-mCherry, and OmpA(1–199 aa)-mCherry, which were integrated into the genome of probiotic *E. coli* Nissle 1917 (EcN) by the Red/ET method (Figure 1A).[20] Therefore, we obtained engineered EcN that secreted mCherry in the lumen of the OMV stably (Figure S1). Then, the fluorescence intensity of the three different mCherry expression patterns were tested using 40 μg of OMVs. The engineered strains were cultured for 16 h at 37°C, and OMVs were purified. OMVs secreted by EcN (WT-OMVs) were used as the control. All the fermentations were carried out in triplicate. The fluorescence intensity of OMVs using the OmpA (1–199 aa)-mCherry expression pattern (OLm-OMVs) was approximately two times of that using LPP-SP+C-mCherry (LSm-OMVs) and 15 times of the OmpA-SP-mCherry (OSm-OMVs) expression pattern (Figure 1B). As proteinase K (PK) can remove proteins on the vesicle surface, the fluorescence intensity of OLm-OMV did not change significantly (Figure S2), indicating that the proteins on the OLm-OMVs mainly consisted of luminal proteins (Figure 1A). To further improve the yield of OMVs, we knocked out the *nlpI* gene and generated the strain EcN-NM (Figure S3).[21] The fluorescence intensity analysis indicated that knocking-out the *nlpI* gene did not affect the loading of mCherry (Figure 1C). Transmission electron microscopy images (Figure 1D) and dynamic light scattering analysis (DLS) (Figure 1E) revealed that engineering the OMVs did not change the morphology and the particle size. In summary, these results demonstrated that mCherry expressed in the lumen of EcN-NM OMVs preserved its functional conformation.

OMVs were engineered with mCherry in the outer membrane and GFP in the lumen

To expand the biological applications of OMV, we considered whether another antigen could be loaded onto the surface of OLm-OMV. Therefore, we used GFP as the model antigen and constructed engineered OMVs loading two antigens (mG-OMV) (Figure 2A). We created a fused gene carrying *clyA* sequence

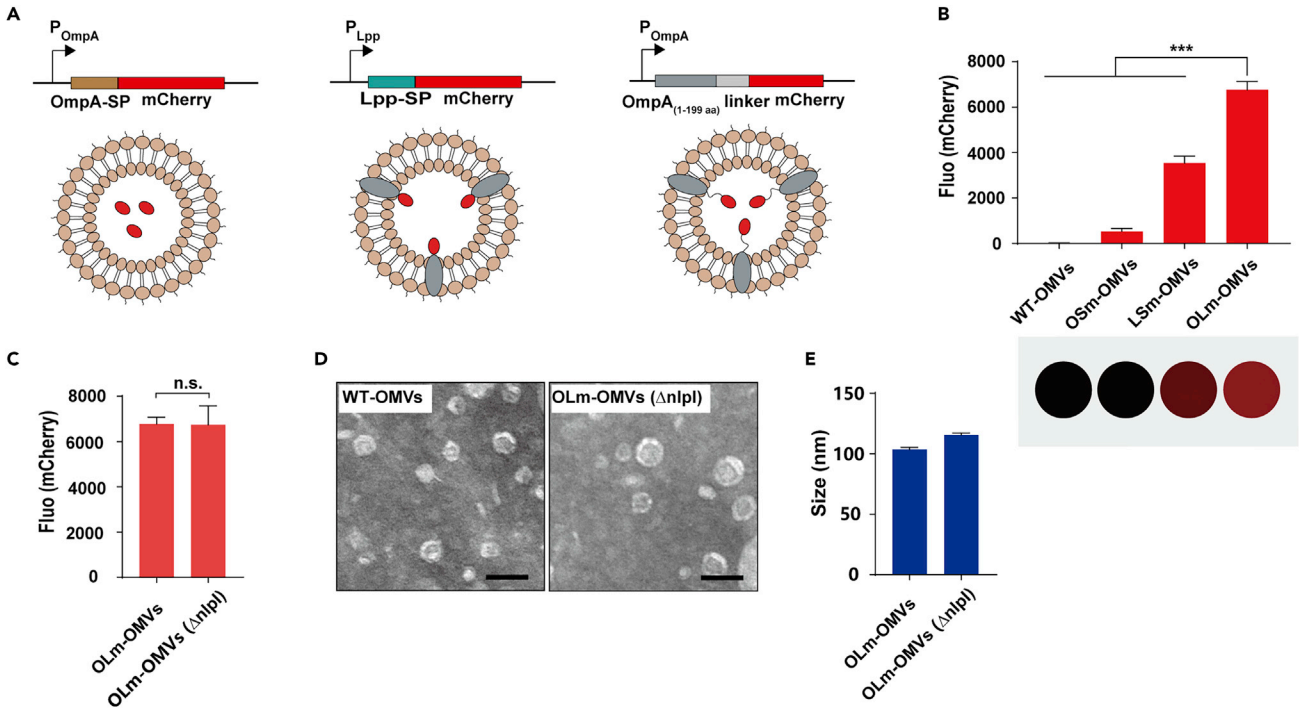

Figure 1. Expression of mCherry in the lumen of OMVs

(A) Schematic design of OmpA-SP-mCherry, Lpp-SP+C-mCherry and OmpA (1–199 aa)-mCherry fusion constructs. Relevant parts of the constructs include the Lpp signal peptide fragment (green), linkers (white), OmpA (1–199 aa) fragment (gray), and the signal peptide of OmpA (orange) and the mCherry (red).

(B) Fluorescence intensity analysis of OmpA-SP-mCherry-OMVs (OSm-OMVs), Lpp-SP+C-mCherry-OMVs (LSm-OMVs), and OmpA (1–199 aa)-mCherry-OMVs (OLm-OMVs). WT-OMV was used as a control, and all samples were loaded with 40 μg for analysis. All experiments were carried out in triplicate. Excitation wavelength: 580 nm; Emission wavelength: 620 nm; ***p = 0.0003. The colored dots represented fluorescence photos observed and taken by a fluorescence microscope, which corresponded to the four groups in the bar chart.

(C) Fluorescence intensity analysis of OLm-OMVs and OLm-OMVs (Δ*nlp*I); 40 μg of all samples were loaded for analysis. All the fermentations were carried out in triplicate. Excitation wavelength: 580 nm; Emission wavelength: 620 nm; N.S. indicates no significance.

(D) TEM analysis of WT-OMVs and OLm-OMVs. Scale bar, 40 nm.

(E) DLS analysis of OLm-OMVs and OLm-OMVs (Δ*nlp*I). OLm-OMVs had a mean diameter of 103.3 nm, and OLm-OMVs (Δ*nlp*I) had similar particle size distribution, with a mean size of 115.1 nm (n = 3). The error bar represents the standard deviations of three independent experiments. The data (B, C) are shown as mean ± SD. Statistical analysis was performed by a two-tailed unpaired *t*-test.

followed by the *gfp* gene. The fused gene was cloned under the control of the arabinose-induced promotor in plasmid pBAD24,[10] and the plasmid was transformed into EcN-NM to generate EcN-mG. OMVs were purified from the culture supernatants. Western blot analysis revealed that the molecular weight of the ClyA-GFP and OmpA (1–199 aa)-mCherry fusions were about 61 kDa and 46 kDa, respectively, which were consistent with our predicted results (Figure 2B). The western-blot analysis indicated that mG-OMVs were successfully decorated with mCherry and GFP. Of note, the fluorescence intensity analysis of mG-OMVs confirmed that displaying GFP on the surface of OLm-OMVs did not interfere with the function of mCherry in the lumen (Figure 2C). To provide direct evidence that GFP was displayed on the surface of OLm-OMVs and mCherry expressed in its lumen, we treated mG-OMVs with PK and found that only the red fluorescence of mCherry could be observed (Figure 2C). Again, transmission electron microscopy images (Figure 2D) and DLS analysis (Figure 2E) revealed that the modification on the surface of OLm-OMVs did not change the morphology and the particle size. In summary, we successfully constructed a dual antigen delivery platform that carried antigens onto the surface of OMVs and into the OMV lumen.

Co-expression of the SARS-CoV-2 receptor-binding domain antigen (RBD) in the OMV outer membrane and the core peptide of RBD (NG06) in the OMV lumen were in their natural conformation

According to previous reports, antigens exposed on the OMV surface probably are easy for antigen-specific B cell binding, whereas luminal antigens hinder the process of their recognition.[22] Therefore, we

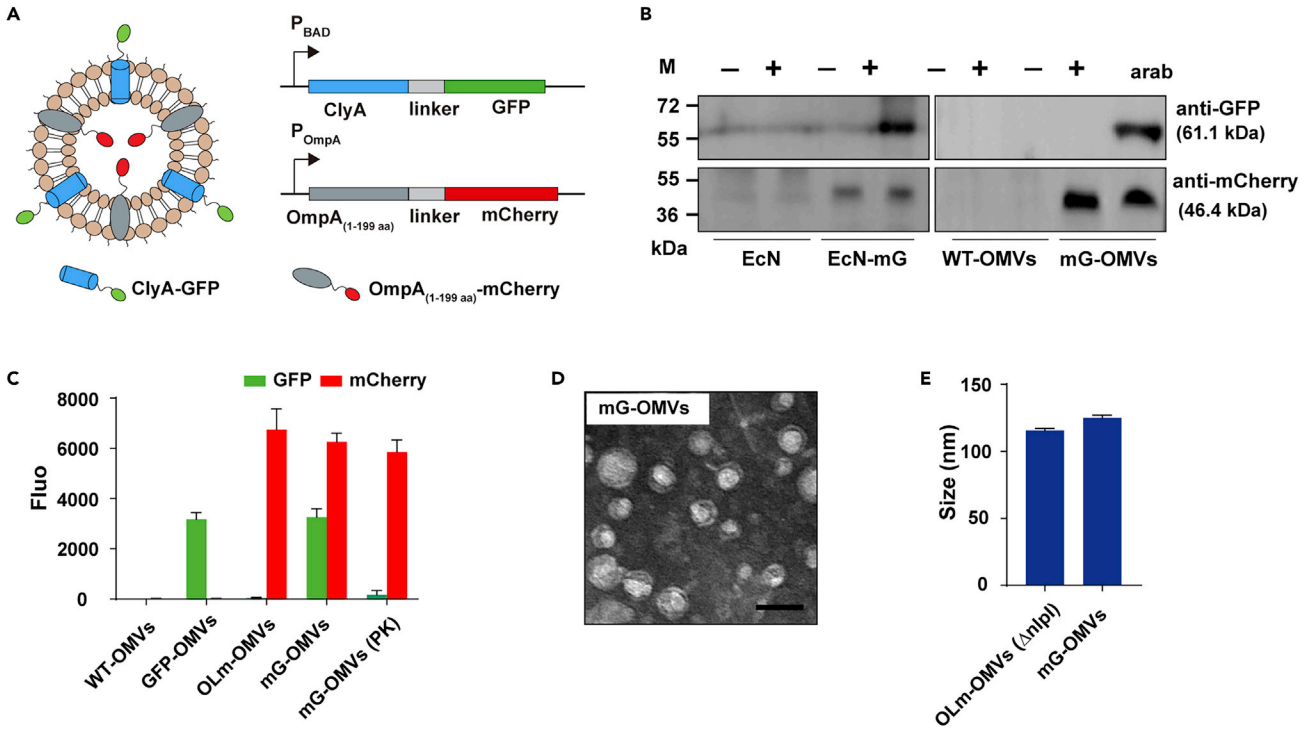

Figure 2. Engineered OMVs with mCherry on the surface and GFP in the lumen

(A) Schematic design of mG-OMV. Relevant parts of the constructs include the GFP (green), linkers (white), OmpA (1–199 aa) fragment (gray), the ClyA (blue), and mCherry (red).

(B) Western blotting of mG-OMVs probed with anti-GFP and anti-mCherry antibodies with or without the addition of 30 mM arabinose. As control, antigen expression was assessed in total cell lysates (EcN and EcN-mG) and was visualized using anti-GFP and anti-mCherry antibodies.

(C) Fluorescence intensity analysis of GFP-OMVs, OLm-OMVs, mG-OMVs, and mG-OMVs treated by Proteinase K. WT-OMVs was used as control, and 40 μg of all samples were loaded for analysis. All experiments were carried out in triplicate. Excitation wavelength (mCherry): 580 nm; Emission wavelength (mCherry): 620 nm; Excitation wavelength (GFP): 488 nm; Emission wavelength (GFP): 528 nm;

(D) TEM analysis of mG-OMVs. Scale bar, 40 nm.

(E) DLS analysis of OLm-OMVs (Δ*nlpI*) and mG-OMVs. The error bar represents the standard deviations of three independent experiments. OLm-OMV had a mean diameter of 115.1 nm, and mG-OMV had similar particle size distribution, with a mean size of 125.1 nm (n = 3). The error bar represents the standard deviations of three independent experiments.

constructed a ClyA-RBD fusion on the OMV surface at first. However, we hardly detected RBD antigen by western blot analysis (Figure S6), the result agreed with a report by Yang *et al.*[23] Fusing ClyA-RBD on the OMV surface failed to achieve the natural conformation of RBD, the result could be explained that *E. coli* cytoplasm did not provide a favorable environment for the expression of RBD.[24] Unlike the cytoplasm, the periplasm of *E. coli* with the Dsb system that catalyzes the formation of disulfide bonds and various chaperones, which facilitate the correct folding of recombinant proteins, was recognized as a high-quality protein expression space.[25–27] To ensure efficient translocation of the SARS-CoV-2 RBD domain to OMVs, we adapted the periplasmic expression strategy (Figure S4). Theoretically, to induce an effective immune response, we selected the NG06 antigen,[28] an immunogenic RBD non-glycosylated region and displayed it efficiently on the surface of RBD-OMVs to obtain NR-OMVs. Using the mG-OMV presentation mode, NR-OMVs carried an internal RBD antigen and displayed the NG06 antigen on their surface (Figures 3A and S5). Western blot analysis confirmed that RBD and NG06 were detected at the expected molecular weight of approximately 44 kDa and 40 kDa, respectively, using NR-OMVs secreted from EcN-NR with 30 mM arabinose addition, and not for WT-OMVs and NR-OMVs secreted from EcN-NR without arabinose (Figure 3B). ELISA analysis demonstrated that compared with WT-OMVs, NR-OMVs elicited higher affinity with the RBD antibody, indicating that the NG06 antigen on the surface of NR-OMVs could be recognized by the RBD antibody (Figure 3C). After ultrasonic treatment, NR-OMVs increased the binding rate with RBD antibody, which resulted from the release of RBD antigen in the NR-OMVs lumen (Figure 3D). The above data indicated that NG06 and RBD could bind to RBD antibodies. Transmission electron microscopy images and NTA analysis demonstrated that the modification on the surface of NR-OMVs did not influence the

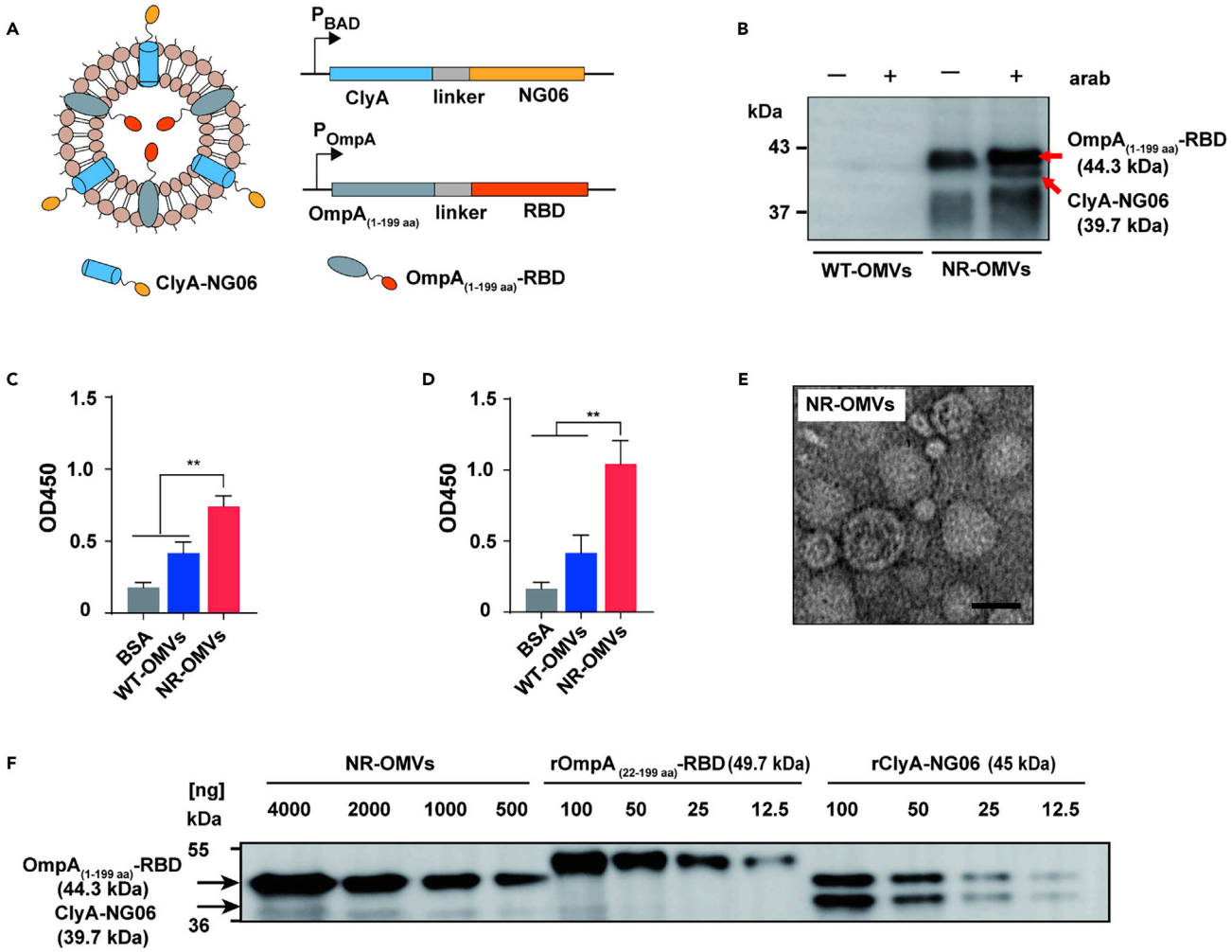

Figure 3. Characterization of NR-OMV

(A) Schematic design of NR-OMV. Relevant parts of the constructs include the NG06 (yellow), linkers (white), OmpA (1–199 aa) fragment (gray), the ClyA (blue), and the RBD (orange).

(B) Western blotting of NR-OMVs probed with an anti-RBD antibody with or without the addition of 30 mM arabinose. WT-OMV group was analyzed as a control.

(C) ELISA analysis of WT-OMV or NR-OMV binding to RBD antibody. All experiments were carried out in triplicate. **p = 0.0062.

(D) ELISA analysis of lysed WT-OMV or NR-OMV binding to RBD antibody. **p = 0.0063. All experiments were carried out in triplicate.

(E) TEM analysis of NR-OMVs. Scale bar, 40 nm. The error bar represents the standard deviations of three independent experiments. The data (C, D) are shown as mean ± SD. Statistical analysis was performed by a two-tailed unpaired *t*-test.

(F) Estimation of the amount of RBD and NG06 incorporated into NR-OMVs by Western blotting analysis. Purified OmpA-RBD and ClyA-NG06 were loaded as standard controls. The percentages of RBD and NG06 in the OMVs were about 5% and 0.5% of total OMV proteins, respectively.

morphology and the particle size was about 148.5 nm (3.3×10^{11} per mL) (Figures 3E and S9). In addition, the amounts of RBD and NG06 in the total OMV proteins were analyzed by western blotting. OmpA-RBD and ClyA-NG06 used as standard controls were expressed by pET28a (+)-his$_6$-OmpA (1–199 aa)-RBD and pBAD24-ClyA-NG06 respectively. By comparing band intensities, RBD and NG06 were estimated at 5% and 0.5% of total OMV proteins, respectively (Figure 3F). Taken together, RBD-antigen was integrated into the OMV lumen in a natural conformation, whereas NG06 was loaded on the surface of RBD-OMVs.

NR-OMVs stimulate BMDC maturation

Dendritic cells (DCs) serve as antigen-presenting cells at the center of immune signaling. After engulfing antigens, the antigens combine with the major histocompatibility complex (MHC) for presentation to T lymphocytes, which promotes DC maturation. Then, the mature DCs upregulate the costimulatory molecules

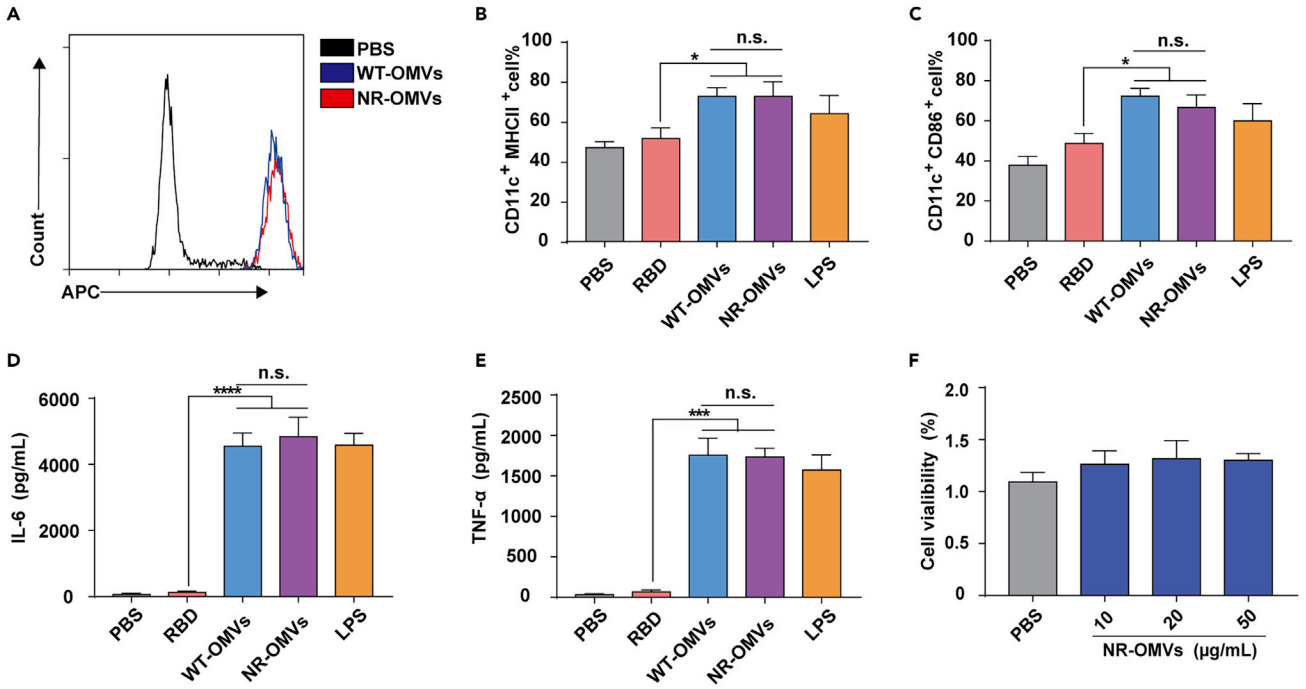

Figure 4. NR-OMVs promoted antigen uptake and BMDC maturation

(A) The rate of DC2.4 uptake was measured by flow cytometry 4 h after adding DID-labeled WT-OMVs and NR-OMVs, PBS served as control.

(B) Flow cytometry analysis of the proportions of CD11c+ and MHCII+ cells 12 h after immature BMDC incubation with either PBS, 0.24 mg/mL LPS,100 ng/mL RBD-antigen, 25 μg/mL WT-OMV, 25 μg/mL NR-OMV. The stimulated BMDC cells were mixed with FITC-anti-mouse-MHC-II, PE-anti-mouse-CD11c for 1 h. *$p < 0.05$. N.S. indicates no significance.

(C) Flow cytometry analysis of the proportions of CD11c+ and $CD86^+$ cells 12 h after immature BMDC incubation with PBS, 0.24 mg/mL LPS, 100 ng/mL RBD-antigen, 25 μg/mL WT-OMV, 25 μg/mL NR-OMV respectively. The stimulated BMDC cells were mixed with PE-anti- mouse-CD11c and APC-anti-mouse-CD86 for 1 h. *$p < 0.05$. N.S. indicate no significance.

(D) The cell culture supernatant was collected to quantify the secretion of IL-6 (D) and TNF-α

(E) by using an ELISA Kit. ****$p < 0.0001$.***$p = 0.0002$. N.S. indicate no significance.

(F) DC2.4 cells were incubated with WT-OMVs or NR-OMVs for 24 h, the cell viability was evaluated by a CCK8 Kit, and cells treated with PBS were used as control. The error bar represents the standard deviations of three independent experiments. The data (B, C, D, E) are shown as mean ± SD. Statistical analysis was performed by a two-tailed unpaired *t*-test.

MHC-II and CD86 expression on their plasma membrane and increase secretion of proinflammatory cytokines (i.e., interleukin (IL) 6, IL1β, and tumor necrosis factor (TNF-α).[29] To test whether modification affects the cellular association of NR-OMVs with DCs, either phosphate-buffer saline (PBS), DID-labeled WT-OMVs, or DID-labeled NR-OMVs were incubated with DC2.4 for 4 h, and the cells were analyzed by flow cytometry. Furthermore, we also tested the cell association of the various OMVs at some earlier time points (30 min and 1 h). The results indicated that WT-OMVs and NR-OMVs shared a similar cellular association with DC2.4 (Figures 4A and S7). Then, immature BMDCs were cultured with either PBS, RBD-antigen, WT-OMVs, NR-OMVs, or lipopolysaccharide (LPS) for 24 h. OMVs are natural immune adjuvants, therefore, we observed that the proportion of CD86 and MHC-II cells showed a significant increase in WT-OMVs and NR-OMVs, and their proportion was higher than the RBD-antigen or PBS group. Also, WT-OMVs and NR-OMVs shared a similar cellular association to BMDCs (Figures 4B and 4C and S8). After antigen stimulation, we further measured TNF-α and IL-6 secreted by mature BMDCs, and both increased significantly (Figures 4D and 4E). In addition, we observed that appropriate concentrations of OMVs did not affect cellular activity (Figure 4F). In conclusion, all results demonstrated that WT-OMVs and NR-OMVs were similar in terms of DC uptake and maturation, and these results indicated that genetic engineering did not affect the immune activation capacity of OMVs.

Synergistic immunogenicity of NR-OMVs

Mice were immunized intraperitoneally (i.p.) three times on days 0, 10, and 20 to evaluate whether the immunization with NR-OMVs could induce humoral immune responses. Mice were injected with 10 μg

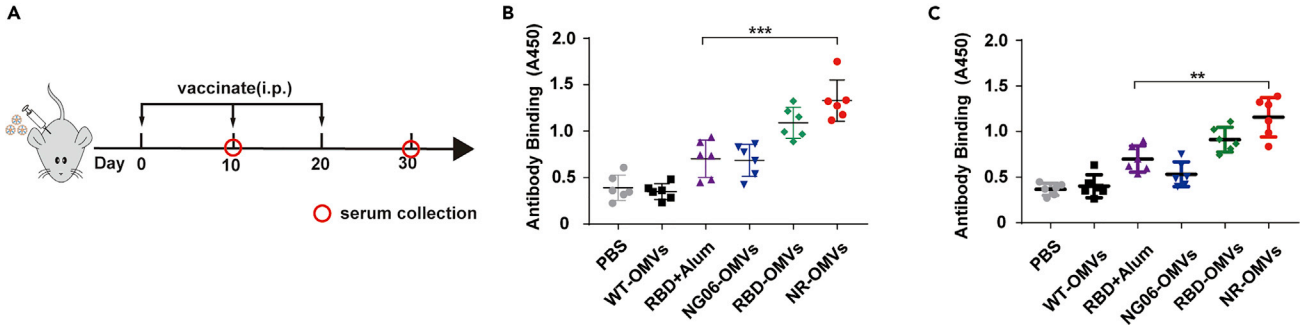

Figure 5. The immunogenicity of NR-OMVs in mice was significantly enhanced compared to NG06-OMVs and RBD-OMVs

(A) Mouse immunization strategy and mouse serum collection point.

(B) Comparison of the immunogenicity of NG06-OMVs, RBD-OMVs, NR-OMVs, and RBD+Alum. Aluminum hydroxide (Alum) is the standard clinical adjuvant. Scatter dot plots represent individual host anti-RBD IgG titers. Serum was collected and diluted at 1:100 on day 10. Groups of six BALB/c mice were immunized with PBS, WT-OMVs, RBD+Alum, NG06-OMVs, RBD-OMVs, and NR-OMVs. ***p = 0.0005.

(C) Comparison of the immunogenicity of WT-OMVs, NG06-OMVs, RBD-OMVs, NR-OMVs, and RBD+Alum. Serum was collected and diluted at 1:1,000 on day 30. Groups of six BALB/c mice were immunized with PBS, WT-OMVs, RBD+Alum, NG06-OMVs, RBD-OMVs, and NR-OMVs. **p = 0.0015. The data (B, C) are shown as the mean ± SD. Statistical analysis was performed by a two-tailed unpaired *t*-test.

OMVs (approximately 0.5 μg and 0.05 μg of RBD and NG06, respectively, were incorporated into OMVs) per immunization, and six immunization groups, including PBS, WT-OMV, NG06-OMV, RBD-OMV, NR-OMV, and RBD+Alum, were tested (Figure 5A). Among them, PBS and WT-OMV served as controls. We monitored the immune responses in sera of immunized mice by ELISA. Sera from days 10 and 30 were used to measure RBD-specific IgG titers against RBD. The titer of RBD antibodies induced by six immunization groups was detected with 100 and 1,000-fold dilutions at two time points. Compared to the control groups, the groups receiving NR-OMV immunization showed a marked increase in IgG titers against RBD for both time points.

In contrast to the NR-OMV immune response, the RBD+Alum immunization group showed low IgG titers against RBD. The antibody titer of the NR-OMV immunization group was 10^3 at day 30, which was about 2.2 times compared to the NG06-OMV immunization group, 1.3 times that of the RBD-OMV immunization group, and 1.7 times that of the traditional vaccine form (RBD+Alum). In conclusion, immunization with NR-OMVs induced a strong antibody response against RBD, which was superior to that of the conventional method, and we found that the loading of NG06 on the surface of OMVs showed synergistic immunogenicity.

DISCUSSION

The RBD of the SARS-CoV-2 spike protein can bind to angiotensin-converting enzyme 2 (ACE2) on the surface of cells, which causes viral invasion.[30] Therefore, the RBD is considered a crucial subunit vaccine target.[31] However, there are two potential glycosylated modification sites (N331 and N343) in the RBD,[24] and because of the lack of post-translational modifications in the bacterial expression system, the mammalian expression systems were considered a promising SARS-CoV-2 vaccine expression platform.[32] OMVs possess built-in adjuvant properties, making them highly suitable as vaccine delivery carriers. Unfortunately, the expression of RBD in the prokaryotic cytoplasm formed inclusions.[33] In addition, we found that the efficiency of displaying RBD on the OMV surface was extremely low (Figure S6), consistent with the existing report.[23] To improve the production of artificial vesicles, Yang et al. used high pressure homogenization technology to drive a bacterial biomimetic vesicle decorated with polymerized ClyA-RBD secretion.[23] Alternatively, a semisynthetic method was adapted to explore an OMV-based vaccine platform, such as Hbp-displaying OMV, which combined a Hbp carrier with a Tag/Catcher protein ligation system.[34] The semisynthetic method elicited relatively high immune responses because the RBD antigen with functional structure was purified from the eukaryotic expression system separately.[34] This study explored and evaluated a novel probiotic-derived OMV vaccine delivery system, which stimulated a significant immune response against the RBD of the SARS-CoV-2 spike protein. This delivery platform purified the engineered NR-OMV without further manipulation, and NR-OMVs elicited robust immune responses.

The above result was probably attributed to the periplasmic expression of RBD. On the one hand, displaying antigens on the surface of OMV is easy for antigen-specific B cell binding, which plays an important role in triggering an antigen-specific immune response.[22] However, displaying ClyA-RBD fusion on the surface of OMV was unsuccessful (Figure S6). On the other hand, unlike prokaryotic cytoplasm, the prokaryotic periplasmic space provides the enzymatic and oxidative conditions required for protein folding and disulfide bond formation, which significantly ensures the quality of the protein after folding, and the signal peptides with different secretion mechanisms can be selected to assist in the secretion of different proteins according to their expression and secretion characteristics.[25–27] As periplasmic proteins are naturally wrapped in OMVs during vesicle formation, periplasmic expression was considered to be an effective method to express proteins required for oxidative conditions.

The OmpA signal peptide is a typical general secretory pathway (Sec) that guides antigen incorporation into the OMV lumen.[35] In addition, OmpA deletions or truncations can generate a blebbing phenotype and increase the production of OMVs.[1] Leveraging the advantages of periplasmic proteins, we designed three luminal fusion expression patterns using mCherry as the model antigen, which was facilitated to test the efficiency of luminal protein expression. We found that RBD-OMVs using the same expression pattern induced the desired immune response.

However, it is controversial whether antigens expression in the OMV lumen is as effective as surface antigens in inducing antigen-specific responses, for their localization prevents direct access by immune effectors.[36] Therefore, we constructed the ClyA-NG06 fusion on the surface of RBD-OMVs and generated NR-OMVs. The result demonstrated that NR-OMVs induced a higher antibody response than RBD-OMVs. The combined results of the immunogenicity of OMVs in mice and the relative amount of RBD (or NG06) in the OMVs, implied that loading NG06 on the surface of RBD-OMVs enhanced immunogenicity (Figures 3F and S10).

In this study, OMVs were secreted by probiotic EcN or its derivative strains. According to the literature report, probiotic derived OMVs balanced the functions of the host immune cells, for instance, by modulating anti-inflammatory and proinflammatory responses.[37] However, OMV-based vaccine candidates also had to balance their adjuvanticity and immunogenicity against their reactogenicity and safety. In work by Zanella et al., the proteome of OMV from *Escherichia coli* BL21 (DE3) was minimized to generate $OMVs_{\Delta 60}$, which deleted 59 endogenous proteins from OMVs. This diverted less attention of the immune system and the engineered $OMVs_{\Delta 60}$ with heterologous antigens enhanced antigen-specific immune response.[38] Hirayama et al. revealed that glycine could dramatically enhance the production of EcN membrane vesicles and that the endotoxin activity was lower than in non-glycine-induced vesicles.[39] In future work, we will concentrate on improving the immunogenicity and safety of the OMVs.

Besides, we constructed a ClyA-NG06 fusion gene on an inducible plasmid that imposed a metabolic burden on EcN or its derivative strains. Recently, Seco et al. established a markerless and scarless method to integrate genes in the chromosome of EcN by bacterial conjunction.[40] In the next study, we plan to express target antigens in the chromosome of EcN by using a markerless and scarless method, which can help us to accumulate multiple antigens in the OMV without the limitation imposed by plasmids. This method circumvents some problems resulting from the use of plasmids, for instance, the exacerbation of metabolic burden, the loss of plasmids without the addition of antibiotics, and the limitation of selection markers. Exploring a genetically stable and low-cost multiple antigen OMV-based platform is important for the biological applications of OMVs in the future.

In conclusion, we developed an engineered OMV-based vaccine candidate delivery platform. Using the OMV-based carrier, we expressed the RBD of SARS-CoV-2 spike protein in the OMV lumen and triggered relatively high immunogenicity. With the ClyA-NG06 fusion displayed on the surface of RBD-OMV, the immunogenicity and antibody titers were enhanced.

Limitations of the study

We developed and evaluated a probiotic-derived vaccine delivery system. However, a principal limitation in this study is that the new vaccine delivery carrier applied to SARS-CoV-2 was only one example. In future work, we will extend this delivery carrier to more examples and provide more detailed information of this delivery carrier.

STAR★METHODS

Detailed methods are provided in the online version of this paper and include the following:

- KEY RESOURCES TABLE
- RESOURCE AVAILABILITY
  - Lead contact
  - Materials availability
  - Data and code availability
- EXPERIMENTAL MODEL AND SUBJECT DETAILS
  - Mice and culture conditions
  - Bacterial strains, cell lines and culture conditions
- METHOD DETAILS
  - Construction of plasmids and deletion mutants
  - Preparation of OMVs
  - Western blot analysis
  - Fluorescence analysis of OMVs
  - Size measurement
  - Nanoparticle tracking analysis
- PROTEINASE K TREATMENT ASSAY
  - Acquisition and maturation of BMDCs
  - Mouse immunization
  - *In vitro* cytotoxicity
  - ELISA
  - Cellular uptake experiments
  - Statistical analysis

SUPPLEMENTAL INFORMATION

Supplemental information can be found online at https://doi.org/10.1016/j.isci.2022.105772.

ACKNOWLEDGMENTS

This study was supported by grants from the National Key Research and Development Program of China (2020YFA0908800) and the National Natural Science Foundation of China (22134003, 31730004).

AUTHOR CONTRIBUTIONS

J.W. and Z.Y.L. conceived, designed, and analyzed all experiments. J.W., Z.Y.L., J.N.S., H.T. conducted experiments. J.W., N.Q., and Z.Y.L. wrote the manuscript. B.C.Y. organized, supervised, and discussed the experiments with J.W. and wrote the manuscript.

DECLARATION OF INTERESTS

The authors declare no competing interests.

INCLUSION AND DIVERSITY

We support inclusive, diverse, and equitable conduct of research.

Received: May 12, 2022
Revised: November 10, 2022
Accepted: December 5, 2022
Published: January 20, 2023

REFERENCES

1. Schwechheimer, C., and Kuehn, M.J. (2015). Outer-membrane vesicles from Gram-negative bacteria: biogenesis and functions. Nat. Rev. Microbiol. *13*, 605–619. https://doi.org/10.1038/nrmicro3525.

2. Toyofuku, M., Nomura, N., and Eberl, L. (2019). Types and origins of bacterial membrane vesicles. Nat. Rev. Microbiol. *17*, 13–24. https://doi.org/10.1038/s41579-018-0112-2.

3. Brown, L., Wolf, J.M., Prados-Rosales, R., and Casadevall, A. (2015). Through the wall: extracellular vesicles in Gram-positive bacteria, mycobacteria and fungi. Nat. Rev. Microbiol. *13*, 620–630. https://doi.org/10.1038/nrmicro3480.

4. Sartorio, M.G., Pardue, E.J., Feldman, M.F., and Haurat, M.F. (2021). Bacterial outer membrane vesicles: from discovery to applications. Annu. Rev. Microbiol. *75*, 609–630. https://doi.org/10.1146/annurev-micro-052821-031444.

5. Dhital, S., Deo, P., Stuart, I., and Naderer, T. (2021). Bacterial outer membrane vesicles and host cell death signaling. Trends Microbiol. *29*, 1106–1116. https://doi.org/10.1016/j.tim.2021.04.003.

6. Kaparakis-Liaskos, M., and Ferrero, R.L. (2015). Immune modulation by bacterial outer membrane vesicles. Nat. Rev. Immunol. *15*, 375–387. https://doi.org/10.1038/nri3837.

7. Gerritzen, M.J.H., Martens, D.E., Wijffels, R.H., van der Pol, L., and Stork, M. (2017). Bioengineering bacterial outer membrane vesicles as vaccine platform. Biotechnol. Adv. *35*, 565–574. https://doi.org/10.1016/j.biotechadv.2017.05.003.

8. Watkins, H.C., Rappazzo, C.G., Higgins, J.S., Sun, X., Brock, N., Chau, A., Misra, A., Cannizzo, J.P.B., King, M.R., Maines, T.R., et al. (2017). Safe Recombinant Outer Membrane Vesicles that Display M2e Elicit Heterologous Influenza Protection. Mol. Ther. *25*, 989–1002. https://doi.org/10.1016/j.ymthe.2017.01.010.

9. Wai, S.N., Lindmark, B., Söderblom, T., Takade, A., Westermark, M., Oscarsson, J., Jass, J., Richter-Dahlfors, A., Mizunoe, Y., and Uhlin, B.E. (2003). Vesicle-mediated export and assembly of pore-forming oligomers of the enterobacterial ClyA cytotoxin. Cell *115*, 25–35. https://doi.org/10.1016/s0092-8674(03)00754-2.

10. Chen, D.J., Osterrieder, N., Metzger, S.M., Buckles, E., Doody, A.M., DeLisa, M.P., and Putnam, D. (2010). Delivery of foreign antigens by engineered outer membrane vesicle vaccines. Proc. Natl. Acad. Sci. USA *107*, 3099–3104. https://doi.org/10.1073/pnas.0805532107.

11. Daleke-Schermerhorn, M.H., Felix, T., Soprova, Z., ten Hagen-Jongman, C.M., Vikström, D., Majlessi, L., Beskers, J., Follmann, F., de Punder, K., van der Wel, N.N., et al. (2014). Decoration of outer membrane vesicles with multiple antigens by using an autotransporter approach. Appl. Environ. Microbiol. *80*, 5854–5865. https://doi.org/10.1128/AEM.01941-14.

12. Fantappiè, L., de Santis, M., Chiarot, E., Carboni, F., Bensi, G., Jousson, O., Margarit, I., and Grandi, G. (2014). Antibody-mediated immunity induced by engineered *Escherichia coli* OMVs carrying heterologous antigens in their lumen. J. Extracell. Vesicles *3*, 24015. https://doi.org/10.3402/jev.v3.24015.

13. Kulp, A., and Kuehn, M.J. (2010). Biological functions and biogenesis of secreted bacterial outer membrane vesicles. Annu. Rev. Microbiol. *64*, 163–184. https://doi.org/10.1146/annurev.micro.091208.073413.

14. Nikaido, H. (2003). Molecular basis of bacterial outer membrane permeability revisited. Microbiol. Mol. Biol. Rev. *67*, 593–656. https://doi.org/10.1128/MMBR.67.4.593-656.2003.

15. Pautsch, A., and Schulz, G.E. (1998). Structure of the outer membrane protein A transmembrane domain. Nat. Struct. Biol. *5*, 1013–1017. https://doi.org/10.1038/2983.

16. Carvalho, A.L., Fonseca, S., Miquel-Clopés, A., Cross, K., Kok, K.S., Wegmann, U., Gil-Cordoso, K., Bentley, E.G., Al Katy, S.H.M., Coombes, J.L., et al. (2019). Bioengineering commensal bacteria-derived outer membrane vesicles for delivery of biologics to the gastrointestinal and respiratory tract. J. Extracell. Vesicles *8*, 1632100. https://doi.org/10.1080/20013078.2019.1632100.

17. Irene, C., Fantappiè, L., Caproni, E., Zerbini, F., Anesi, A., Tomasi, M., Zanella, I., Stupia, S., Prete, S., Valensin, S., et al. (2019). Bacterial outer membrane vesicles engineered with lipidated antigens as a platform for *Staphylococcus aureus* vaccine. Proc. Natl. Acad. Sci. USA *116*, 21780–21788. https://doi.org/10.1073/pnas.1905112116.

18. Okuda, S., and Tokuda, H. (2011). Lipoprotein sorting in bacteria. Annu. Rev. Microbiol. *65*, 239–259. https://doi.org/10.1146/annurev-micro-090110-102859.

19. Smithers, L., Olatunji, S., and Caffrey, M. (2021). Bacterial lipoprotein posttranslational modifications. New insights and opportunities for antibiotic and vaccine development. Front. Microbiol. *12*, 788445. https://doi.org/10.3389/fmicb.2021.788445.

20. Sharan, S.K., Thomason, L.C., Kuznetsov, S.G., and Court, D.L. (2009). Recombineering: a homologous recombination-based method of genetic engineering. Nat. Protoc. *4*, 206–223. https://doi.org/10.1038/nprot.2008.227.

21. McBroom, A.J., and Kuehn, M.J. (2007). Release of outer membrane vesicles by Gram-negative bacteria is a novel envelope stress response. Mol. Microbiol. *63*, 545–558. https://doi.org/10.1111/j.1365-2958.2006.05522.x.

22. Necchi, F., Stefanetti, G., Alfini, R., Palmieri, E., Carducci, M., Di Benedetto, R., Schiavo, F., Aruta, M.G., Giusti, F., Ferlenghi, I., et al. (2021). *Neisseria meningitidis* factor H binding protein surface exposure on *Salmonella typhimurium* GMMA is critical to induce an effective immune response against both diseases. Pathogens *10*, 726. https://doi.org/10.3390/pathogens10060726.

23. Yang, Z., Hua, L., Yang, M., Liu, S.Q., Shen, J., Li, W., Long, Q., Bai, H., Yang, X., Ren, Z., et al. (2021). RBD-modified bacterial vesicles elicited potential protective immunity against SARS-CoV-2. Nano Lett. *21*, 5920–5930. https://doi.org/10.1021/acs.nanolett.1c00680.

24. Watanabe, Y., Allen, J.D., Wrapp, D., McLellan, J.S., and Crispin, M. (2020). Site-specific glycan analysis of the SARS-CoV-2 spike. Science *369*, 330–333. https://doi.org/10.1126/science.abb9983.

25. Ke, N., and Berkmen, M. (2014). Production of disulfide-bonded proteins in *Escherichia coli*. Curr. Protoc. Mol. Biol. *108*, 16–21. https://doi.org/10.1002/0471142727.mb1601bs108.

26. Wu, X., Liu, J., Liu, Z., Gong, G., and Zha, J. (2022). Microbial cell surface engineering for high-level synthesis of bio-products. Biotechnol. Adv. *55*, 107912. https://doi.org/10.1016/j.biotechadv.2022.107912.

27. Ytterberg, A.J., Zubarev, R.A., and Baumgarten, T. (2019). Posttranslational targeting of a recombinant protein promotes its efficient secretion into the *Escherichia coli* periplasm. Appl. Environ. Microbiol. *85*. e00671-19. https://doi.org/10.1128/AEM.00671-19.

28. Núñez-Muñoz, L., Marcelino-Pérez, G., Calderón-Pérez, B., Pérez-Saldívar, M., Acosta-Virgen, K., González-Conchillos, H., Vargas-Hernández, B., Olivares-Martínez, A., Ruiz-Medrano, R., Roa-Velázquez, D., et al. (2021). Recombinant antigens based on non-glycosylated regions from RBD SARS-CoV-2 as potential vaccine candidates against COVID-19. Vaccines *9*, 928. https://doi.org/10.3390/vaccines9080928.

29. Lanzavecchia, A., and Sallusto, F. (2001). Regulation of T cell immunity by dendritic cells. Cell *106*, 263–266. https://doi.org/10.1016/S0092-8674(01)00455-X.

30. Zhou, P., Yang, X.L., Wang, X.G., Hu, B., Zhang, L., Zhang, W., Si, H.R., Zhu, Y., Li, B., Huang, C.L., et al. (2020). A pneumonia outbreak associated with a new coronavirus of probable bat origin. Nature *579*, 270–273. https://doi.org/10.1038/s41586-020-2012-7.

31. Pinto, D., Park, Y.J., Beltramello, M., Walls, A.C., Tortorici, M.A., Bianchi, S., Jaconi, S., Culap, K., Zatta, F., De Marco, A., et al. (2020). Cross-neutralization of SARS-CoV-2 by a human monoclonal SARS-CoV antibody. Nature *583*, 290–295. https://doi.org/10.1038/s41586-020-2349-y.

32. Zang, J., Gu, C., Zhou, B., Zhang, C., Yang, Y., Xu, S., Bai, L., Zhang, R., Deng, Q., Yuan, Z., et al. (2020). Immunization with the receptor-binding domain of SARS-CoV-2 elicits antibodies cross-neutralizing SARS-CoV-2 and SARS-CoV without antibody-dependent enhancement. Cell Discov. *6*, 61. https://doi.org/10.1038/s41421-020-00199-1.

33. Su, Q.D., Zou, Y.N., Yi, Y., Shen, L.P., Ye, X.Z., Zhang, Y., Wang, H., Ke, H., Song, J.D., Hu, K.P., et al. (2021). Recombinant SARS-CoV-2 RBD with a built in T helper epitope induces strong neutralization antibody response. Vaccine *39*, 1241–1247. https://doi.org/10.1016/j.vaccine.2021.01.044.

34. Jiang, L., Driedonks, T.A., Jong, W.S., Dhakal, S., Berg van Saparoea, H.B.v.d., Sitaras, I., Zhou, R., Caputo, C., Littlefield, K., Lowman, M., et al. (2022). A bacterial extracellular vesicle-based intranasal vaccine against SARS-CoV-2 protects against disease and elicits neutralizing antibodies to wild-type and Delta variants. bioRxiv *11*, 2021.06.28.450181. https://doi.org/10.1101/2021.06.28.450181.

35. Zhou, Y., Lu, Z., Wang, X., Selvaraj, J.N., and Zhang, G. (2018). Genetic engineering modification and fermentation optimization

for extracellular production of recombinant proteins using. Appl. Microbiol. Biotechnol. *102*, 1545–1556. https://doi.org/10.1007/s00253-017-8700-z.

36. Zhu, Z., Antenucci, F., Villumsen, K.R., and Bojesen, A.M. (2021). Bacterial outer membrane vesicles as a versatile tool in vaccine research and the fight against antimicrobial resistance. mBio *12*, e0170721. https://doi.org/10.1128/mBio.01707-21.

37. Hu, R., Lin, H., Li, J., Zhao, Y., Wang, M., Sun, X., Min, Y., Gao, Y., and Yang, M. (2020). Probiotic *Escherichia coli* Nissle 1917-derived outer membrane vesicles enhance immunomodulation and antimicrobial activity in RAW264.7 macrophages. BMC Microbiol. *20*, 268. https://doi.org/10.1186/s12866-020-01953-x.

38. Zanella, I., König, E., Tomasi, M., Gagliardi, A., Frattini, L., Fantappiè, L., Irene, C., Zerbini, F., Caproni, E., Isaac, S.J., et al. (2021). Proteome-minimized outer membrane vesicles from *Escherichia coli* as a generalized vaccine platform. J. Extracell. Vesicles *10*, e12066. https://doi.org/10.1002/jev2.12066.

39. Hirayama, S., and Nakao, R. (2020). Glycine significantly enhances bacterial membrane vesicle production: a powerful approach for isolation of LPS-reduced membrane vesicles of probiotic. Microb. Biotechnol. *13*, 1162–1178. https://doi.org/10.1111/1751-7915.13572.

40. Seco, E.M., and Fernández, L.Á. (2022). Efficient markerless integration of genes in the chromosome of probiotic *E. coli* Nissle 1917 by bacterial conjugation. Microb. Biotechnol. *15*, 1374–1391. https://doi.org/10.1111/1751-7915.13967.

41. Roney, K. (2019). Bone marrow-derived dendritic cells. Methods Mol. Biol. *1960*, 57–62. https://doi.org/10.1007/978-1-4939-9167-9_4.

STAR★METHODS

KEY RESOURCES TABLE

REAGENT or RESOURCE	SOURCE	IDENTIFIER
Antibodies		
SARS-CoV-2 (2019-nCoV) Spike RBD Antibody	SinoBiological	Cat#40592-T62; RRID: AB_2927483
GFP Tag Monoclonal antibody	Proteintech	Cat#66002-1-Ig; RRID: AB_11182611
mCherry Polyclonal antibody	Proteintech	Cat#26765-1-AP; RRID: AB_2876881
Goat Anti-Rabbit IgG-HRP	Proteintech	Cat#SA00001-2; RRID: AB_2722564
PE Anti-Mouse CD11c	TONBO	Cat#50-0114-U100; RRID: AB_2621747
APC-CD86 Monoclonal Antibody	eBioscience	Cat#17-0862-81; RRID: AB_469418
FITC-MHC Class II Monoclonal Antibody	eBioscience	Cat#11-5321-81; RRID: AB_465231
Bacterial and Virus Strains		
E. coli DH5α	Biobw	Cat#Bio82081
E. coli MG1655	Biobw	Cat#Bio82268
E. coli Nissle 1917	Biobw	Cat#Bio089890
Chemicals, Peptides, and Recombinant Proteins		
Recombinant SARS-CoV-2 Spike RBD protein	Sangon Biotech	Cat#C500304-0001
DiD Cell-Labeling Solution	Thermo Fisher	Cat#V22887
FastDigest *Hind*III	Thermo Fisher	Cat#FD0505
FastDigest *Nco*I	Thermo Fisher	Cat#FD0574
Ammonium molybdate tetrahydrate	Solarbio	Cat#A7120
Phanta Max Super-Fidelity DNA Polymerase	Vazyme	Cat#P505-d1
Proteinase K	TransGen	Cat#GE201-01
phenylmethylsulfonyl fluoride (PMSF)	Beyotime	Cat# ST506
10 × PBS Buffer	Solarbio	Cat#P1002
Protein Ladder	Thermo Fisher	Cat#26617
Albumin bovine serum	Solarbio	Cat#A8010
Lipopolysaccharides (LPS)	Solarbio	Cat#L8880
Fetal Bovine Serum (FBS)	BIOIND	Cat#04-001-1A
RPMI 1640 Medium	Gibco	Cat#11875176
Trypsin-EDTA	Gibco	Cat#25200072
Penicillin-Streptomycin Liquid	Solarbio	Cat#P1400
GM-CSF	PeproTech	Cat#96-315-03–5
IL-4	PeproTech	Cat#96-214-14–5
Red Blood Cell Lysis Buffer	Beyotime	Cat#C3702
Tetramethylbenzidine (TMB)	Solarbio	Cat#T9230
50 × TAE Buffer	Sangon Biotech	Cat#B548101-0500
L-(+)-Arabinose	Sangon Biotech	Cat#A610071-0025
LumiQ HRP Substrate solution	ShareBio	Cat#SB-WB012
Critical Commercial Assays		
Plasmid extraction kit	TIANGEN	Cat#DP103
Gel extraction kit	TIANGEN	Cat#DP219
Hieff Clone® Plus Multi One Step Cloning Kit	YEASEN	Cat#10912ES10
Bacterial MVs Isolation Kit	RENGEN	Cat#BacMv40-10
Mouse TNF-α ELISA KIT	QuantiCyto	Cat#EMC102a

(*Continued on next page*)

Continued

REAGENT or RESOURCE	SOURCE	IDENTIFIER
Mouse IL-6 ELISA KIT	QuantiCyto	Cat#ECM004.96
SARS-CoV-2 (2019-nCoV) Spike RBD Antibody Titer Assay Kit	SinoBiological	Cat#KIT006
Cell Counting Kit (CCK-8)	YEASEN	Cat#40203ES60
BCA Protein Assay Kit	Beyotime	Cat#P0012
Experimental Models: Cell Lines		
BMDC, Plasma of BALB/c	Ziyuan Laboratory Animal Science and Technology Co. Ltd.	N/A
DC 2.4	KeyGEN Biotech	Cat#KG581
Experimental Models: Organisms/Strains		
BALB/c	Ziyuan Laboratory Animal Science and Technology Co. Ltd.	N/A
Oligonucleotides		
For primer sequences see Table S2	This study	N/A
Recombinant DNA		
pBAD-ClyA-GFP	This study	N/A
pBAD-ClyA-NG06	This study	N/A
pBAD-ClyA-RBD	This study	N/A
pBAD24	Miaolingbio	Cat#P0082
pKD46	Miaolingbio	Cat#P0098
pKD3	Miaolingbio	Cat#P0095
pET28a(+)-GFP	Miaolingbio	Cat#P0024
pET28a(+)-mCherry	N/A	N/A
pSET152	N/A	N/A
Software and Algorithms		
GraphPad Prism 7	GraphPad Prism	https://www.graphpad.com/
Adobe Illustrator CC 2014	Adobe	https://www.adobe.com/
Cytexpert	BECKMAN	https://cytexpert.updatestar.com/
Image J	NIH	https://ImageJ.NIH.gov/

RESOURCE AVAILABILITY

Lead contact

Further information and reasonable requests for resources and reagents may be directed to and will be fulfilled by the lead contact, Bang-Ce Ye (bcye@ecust.edu.cn).

Materials availability

All unique/stable reagents generated in this study are available from the lead contact with a completed Materials Transfer Agreement.

Data and code availability

This study did not generate any unique datasets or code.

EXPERIMENTAL MODEL AND SUBJECT DETAILS

Mice and culture conditions

BALB/c female 8-week-old mice were purchased from ZIYUAN Biotechnology Co., Ltd. (Hangzhou, China). Mice were maintained in SPF (Specific pathogen Free, SPF) conditions at 22°C. All animal experiments were

conducted following the guidelines evaluated and approved for laboratory animals at the Zhejiang University of Technology (Approval number: 20211214109)

Bacterial strains, cell lines and culture conditions

Escherichia coli DH5α was used as a sub-cloning host, whereas *E. coli* Nissle 1917 was used as an expression host. Unless stated otherwise, all strains were grown at 37°C in Luria-Bertani medium (10 g/L tryptone, 5 g/L yeast extract, 5 g/L NaCl). If required, antibiotics and other supplements were added, for instance, kanamycin (50 μg/mL), ampicillin (100 μg/mL), and arabinose (30 mM).

DC2.4 cells were cultured in 1640 supplemented with 10% fetal bovine serum, 100 U/mL streptomycin, and 100 U/mL penicillin.

BMDCs were cultured in 1640 media containing 10% fetal bovine serum, 100 U/mL streptomycin, and 100 U/mL penicillin, 50 nM 2-mercaptoethanol, and 20 ng/mL GM-CSF and 10 ng/mL IL-4.[41] One-half of the media was replaced every 2 days. All cells were cultured at 37°C in humidified surroundings with 5% CO_2.

METHOD DETAILS

Construction of plasmids and deletion mutants

Plasmids of pBAD-ClyA-GFP and pBAD-ClyA-NG06 were constructed to display GFP or NG06 on the OMV surface. The *clyA* gene was amplified from *E. coli* MG1655 using primers CG-F1/CG-R1 and CN-F1/CN-R1. The *gfp* gene was amplified from pET28a(+)-GFP using CG-F2/CG-R2. The *ng06* gene was amplified using primers CN-F2/CN-R2. Plasmid pBAD24 was linearized with *Nco*I and *Hin*dIII at 37°C for 30 min. The corresponding PCR products were ligated into pBAD24 to generate pBAD-ClyA-GFP and pBAD-ClyA-NG06 by using a Hieff Clone Plus Multi One Step Cloning Kit (Shanghai, China). Plasmids were transformed into EcN or its derivative strains and positive colonies were selected by PCR analysis.

EcNΔ*nlpI* was constructed by replacing the *nlpI* gene with an apramycin resistance cassette. The upstream and downstream regions of the *nlpI* gene were amplified from the genome of EcN using the primers DN-F1/DN-R1 and DN-F2/DN-R2 (Table S2). The *aac(3)*IV gene was amplified from the pSET152 plasmid using the primers APR-F/APR-R. Finally, the four PCR products were ligated together to generate a linear fragment which was transformed into EcN with pKD46 plasmid by electroporation. Transformed bacteria were plated on LB plates containing 50 μg/mL of apramycin and 100 μg/mL ampicillin at 30°C for 16 h. EcNΔ*nlpI* mutant colonies were confirmed by PCR analysis of genomic DNA using the primer pairs DNT-F/DNT-R (Table S2). The positive colony was incubated at 42°C overnight to promote the loss of temperature-sensitive plasmid pKD46 from EcNΔ*nlpI*.

An EcN-LSm mutant was generated by replacing the *lpp* coding sequence using a chloramphenicol (Cm) resistance cassette. The upstream and downstream arms of the *lpp* gene were amplified from the EcN genomic DNA using the primers LSm-F1/LSm-R1 and LSm-F4/LSm-R4 (Table S2). The *cat* gene was amplified from the pKD3 plasmid using the primers LSm-F3/LSm-R3 (Table S2). The *mcherry* gene was amplified from the pET28a(+)-mCherry plasmid DNA with the primers LSm-F2/LSm-R2 (Table S2). Finally, the four PCR products were ligated together to obtain a linear fragment. The linear fragment was transformed into EcN harboring pKD46 plasmid by electroporation. Transformed bacteria were spread onto LB agar plates containing 25 μg/mL of chloramphenicol and 100 μg/mL ampicillin at 30°C for 16 h. EcN-LSm mutant colonies were confirmed by PCR analysis of genomic DNA using the primer pairs LSmT-F/LSmT-R (Table S2). The positive colonies were cultivated at 42°C overnight to eliminate the temperature-sensitive plasmid pKD46.

The construction procedure of EcN-OSm, EcN-OLm, EcN-OLm (Δ*nlpI*), and EcN-R were similar to EcN-LSm and the corresponding primers are listed in Table S2.

Preparation of OMVs

Strains or mutants were cultivated with or without antibiotics in 200 mL LB at 37°C for 18 h. The mutant harboring the expression plasmid under the control of the P_{BAD} promotor needed to be supplemented with a final concentration of 30 mM arabinose to induce the corresponding protein expression when

OD_{600} reached 0.4–0.6. The culture was incubated further at 37°C for another 15 h. The cells were removed from the supernatant by centrifugation at 10,000 × g for 20 min at 4°C. The supernatant was filtered by a 0.22 μm filter, and then it was concentrated to 20 mL using a 100 kDa ultrafiltration tube. OMVs were purified by an OMV isolation kit. The surface protein concentration of the OMVs was measured by a BCA protein assay kit.

Western blot analysis

Total bacterial protein and OMV suspension were inactivated in boiling water for 15 min after being suspended in an SDS-PAGE loading buffer. Samples were analyzed on 9% or 12% SDS-PAGE and then transferred onto a 0.45 μm polyvinylidene fluoride (PVDF) membrane. The PVDF membranes were blocked by 5% nonfat milk for 90 min at room temperature and incubated with an anti-GFP monoclonal antibody, anti-mCherry polyclonal antibody, or anti-RBD polyclonal antibody overnight at 4°C. After washing three times with TBST (0.05% Tween in TBS), the PVDF membranes were incubated in a 1:2,500 dilution of HRP-conjugated donkey anti-rabbit IgG or HRP-conjugated goat anti-mouse IgG for 1 h. After washing three times with TBST, the immunoreactive proteins were analyzed by adding an HRP substrate solution.

Fluorescence analysis of OMVs

The samples (40 μg of OMVs in 100 μL PBS) were transferred into a 96-well plate and analyzed by using a microplate reader. The fluorescence intensity of GFP was measured at the excitation wavelength of 488 nm and the emission wavelength of 527 nm. The fluorescence intensity of mCherry was measured at the excitation wavelength of 580 nm and an emission wavelength of 620 nm.

Size measurement

The morphological characterization of OMVs was observed with a 120 kv transmission electron microscope. In brief, OMVs were washed three times with PBS by ultrafiltration. Add OMV suspension (10 μL) was added to a copper grid. After 10 min, the OMV samples were completely dried out, then OMVs were stained with 3% ammonium molybdate for 10 min. Finally, the sample was observed by using a 120 kv transmission electron microscope. The size of OMV was measured by dynamic light scattering (DLS). Samples were filtered with a 0.22 μm filter before being measured.

Nanoparticle tracking analysis

Samples were analyzed by the ZetaView PMX110 system according to the instructions of manufacturer. NR-OMVs (0.5 mg/mL) were diluted 1:5,000 in PBS and the total amount of NR-OMV particles was analyzed by ZetaView 8.04.02 SP2 (Particle Metrix, Inning, Germany). The sample was measured three times at room temperature.

PROTEINASE K TREATMENT ASSAY

Proteinase K was incubated with OMVs at a final concentration of 100 μg/mL, and the mixture was incubated at 37°C for 15 min in the presence or absence of 1% SDS. The reaction was terminated with a final concentration of 10 mM phenylmethylsulfonyl fluoride (PMSF).[12] Samples were analyzed by SDS-PAGE and Western Blot using anti-RBD antibodies as described in the following text.

Acquisition and maturation of BMDCs

Femurs and tibias were harvested from 10-week-old BALB/c mice. BMDCs were flushed from tibias and femurs with 1640 media and washed three times. After 5 min of lysis using 5 mL of red blood cell lysis buffer, BMDCs were cultured in 1640 media containing 10% fetal bovine serum, 100 U/mL streptomycin, and 100 U/mL penicillin, 50 nM 2-mercaptoethanol, 20 ng/mL GM-CSF, and 10 ng/mL IL-4. One-half of the media was replaced every two days. All nonadherent cells were harvested for downstream experiments. BMDCs mixed with PBS, LPS (0.24 mg/mL), RBD (100 ng/mL), WT-OMVs (25 μg/mL) or NR-OMVs (25 μg/mL) were cultured in 24-well plates for 12 h. Then, cells were harvested and stained with PE anti-mouse CD11c, APC anti-mouse CD86, FITC anti-mouse MHC-II at 37°C for 60 min and washed with PBS three times. BMDCs were harvested by centrifugation at 2,000 × g for 5 min at 4°C and re-suspended with PBS, which were used to analyze the level of maturation by flow cytometry. The supernatant of the sample was collected, and it was used to analyze the concentration of cytokines IL-6 and TNF-α by ELISA kits. The culture process was performed at 37°C in humidified surroundings with 5% CO_2.

Mouse immunization

For immunization, 8-week-old BALB/c mice were injected intraperitoneally (i.p.) with a dose of 10 μg (total protein content of OMVs) of WT-OMVs (n = 6), 10 μg (total protein content of OMVs) of NG06-OMVs (n = 6), 10 μg (total protein content of OMVs) of RBD-OMVs (n = 6), 10 μg (total protein content of OMVs) of NR-OMVs (n = 6), 2 μg of RBD protein mixed with Alum (n = 6), 100 μL of PBS on days 0, 10, and 20. All drugs were dissolved in 100 μL of PBS. Mice blood were collected on days 10 and 30. The mice were kept pathogen-free with a humidity of 40–60% and at a temperature of 25°C. All animal experiments were conducted following the guidelines evaluated and approved for laboratory animals at the Zhejiang University of Technology (Approval number: 20211214109).

In vitro cytotoxicity

DC2.4 cells were seeded in 96-well plates with about 6000 cells per well. After 12 h of incubation, the cells were cultured with NR-OMVs at different concentrations (10, 20, and 50 μg/mL) for 24 h. The cytotoxicity of NR-OMVs was measured by using a CCK8-kit according to instructions.

ELISA

Diluted WT-OMVs (2 μg/mL), NR-OMVs (2 μg/mL), lysed WT-OMVs (2 μg/mL) and lysed NR-OMVs (2 μg/mL) were added to 96-well plates. Samples were blocked with 100 μL of 1% BSA for 2 h at 4°C. Each well was washed with PBS containing 0.05% Tween-20 5 times. Then the plates were incubated with 100 μL of anti-RBD polyclonal antibody (1:5,000) for 1 h at 37°C. Washed with PBST 5 times and 100 μL/well of 1:2,000 diluted HRP-conjugated donkey anti-rabbit IgG was added for 1 h at 37°C. After five washes, 100 μL of 3,3',5,5' -tetramethylbenzidine (TMB) substrate solution was added to each well for 20 min of incubation. Then, the reaction was stopped by adding 100 μL of H_2SO_4 (0.2 M) and detected at 450 nm using an enzyme-labeled instrument. Mouse sera were successively diluted with PBST and analyzed by using a SARS-CoV-2 (2019-nCoV) Spike RBD Antibody Titer Assay Kit (Sino Biological, Beijing, China).

Cellular uptake experiments

All samples of OMVs were mixed with DiD Cell-Labeling Solutions (Invitrogen) for 30 min and were completely washed with PBS by using a 100 kDa ultrafiltration tube. DC2.4 cells (3×10^4) were plated into a 24-well plate and cultured for 6 h. The cells were then incubated with DID-labeled WT-OMVs and DID-labeled NR-OMVs for 6 h at 37°C. After washing three times with PBS, the cells were harvested by centrifugation at 2,000 g for 5 min at 4°C, which was detected with a flow cytometer.

Statistical analysis

The data presented were performed at least three times. Data were presented as the mean ± SD. Statistical analyses were performed by using GraphPad Prism software version 7.0. The comparison of two groups was analyzed by a two-tailed unpaired *t*-test.